SCIENCE AND TECHNOLOGY OF WELDING AND JOINING, 2016
http://dx.doi.org/10.1080/13621718.2016.1232674

The Institute of Materials, Minerals and Mining

Taylor & Francis
Taylor & Francis Group

# Modified WIC test: an efficient and effective tool for evaluating pipeline girth weldability

R. Kurji[a], N. Coniglio[b], J. Griggs[a] and R. Ghomashchi[a]

[a]School of Mechanical Engineering, The University of Adelaide, Adelaide, Australia; [b]Ecole Nationale Supérieure d'Arts et Métiers ParisTech, Laboratory MSMP, Aix en Provence, France

**ABSTRACT**

The Welding Institute of Canada (WIC) test is a simple and standardised weldability test for hydrogen assisted cold cracking that was developed in the 80s. It has been extensively utilised by the industry to qualify safe welding envelopes but the difficult access to the weldment by instrumentation hinders its use for scientific research. Moreover the lack of repeatability arising from the traditional manual deposit and the short weld length causes industrial trials to have a low success rate. The present work proposes a modified geometry, referred to as the modified WIC (MWIC) test that shows: (1) an improved success rate of weld deposition, (2) an enhancement to instrument the weldment and (3) welding conditions in better accordance with the field pipeline girth welding conditions. The design is validated under a mechanised, shielded metal arc welding process with the cellulosic electrodes used for in-field pipeline construction.

**ARTICLE HISTORY**
Received 16 June 2016
Accepted 25 August 2016

**KEYWORDS**
Hydrogen assisted cold cracking; weldability testing; shielded metal arc welding; modified welding institute of canada

## Introduction

The pipeline industry has long desired the establishment of standardised weldability tests in order to quantify the susceptibility to hydrogen assisted cold cracking (HACC) of pipeline girth welds [1–3], a significant threat to pipeline weld integrity. The predominant advantage of such standardisation is the ability to compare weldability test data across a range of sources reliably and with confidence. This is becoming ever more important as the prevalence of weld metal HACC (WMHACC) is increasing [4–7] and major standards such as the Australian Standards AS2885.2:2007 [8] and the European Standard EN 1011-2:2001 [9] do not provide guidelines on specific procedures such as preheating to minimise the risk of cracking.

HACC is a defect likely to occur in hydrogenated weldments subjected to high residual tensile stresses. HACC is complex in nature, involving interplay between hydrogen and thermal, mechanical and metallurgical factors. A number of theories and criteria have been proposed to describe and characterise HACC formation, as indicated in reviews on the subject [2,5,10–15]. However, since the underlying mechanism governing this phenomenon is not well understood, it is still a contentious subject today.

Hydrogen may be introduced into the weld, during welding, from several sources including contaminants such as oil and grease present on the surface of the weld preps and atmospheric moisture. However, the dominant source of hydrogen when welding is the electrode flux itself. In the root pass of pipeline girth welds where high deposition rates and deep penetration welds are required the use of cellulosic electrodes is common place [16–19]. The disassociation of the cellulosic $(C_6H_{10}O_5)_n$ flux and the moisture it contains during welding introduces into the weld metal larger amounts of diffusible hydrogen ($10^1$–$10^2$ mL $H_2$/100 g Fe) [20]. The development of the tensile residual stress during weld metal cooling provides the complementary driving force for HACC formation [20–23].

Technological advancements in the steel making process have led to the development of higher strength line pipe steel. The economic benefits, including higher capacity and a net cost saving following a reduction in the raw tonnage of steel used, have accelerated its adoption by industry. The use of higher strength steels has necessitated the use of higher strength electrodes for pipeline construction. The richer chemistry of high strength electrodes delays the weld metal austenite-to-ferrite transformation in such a way that the transformation occurs after the austenite-to-ferrite transformation of the HAZ of high strength low alloy (HSLA) steel pipes. As the solubility of hydrogen is lower in ferrite than austenite, hydrogen is rejected during cooling from the ferritic HAZ to the adjacent austenitic weld metal [20]. The subsequent high levels of hydrogen in the weld metal favours the formation of cold cracking into the weld metal.

**CONTACT** R. Kurji rahim.kurji@adelaide.edu.au; R. Ghomashchi reza.ghomashchi@adelaide.edu.au

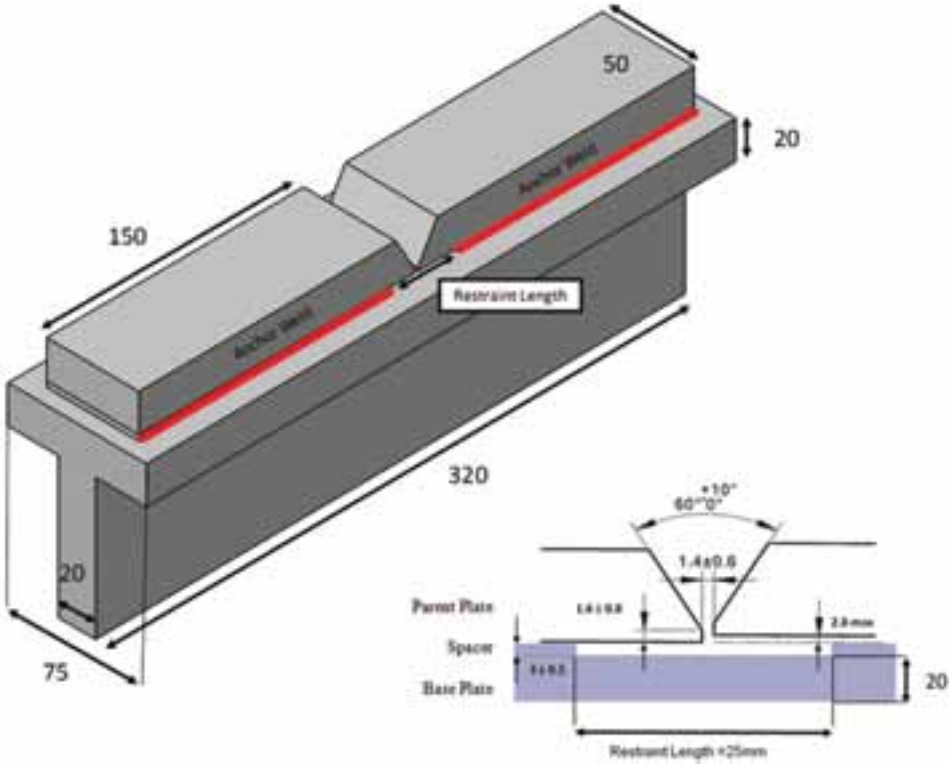


**Figure 1.** Schematic of experimental setup for WIC test.

In such cases (i.e. where HSLA steels are welded with cellulosic electrodes) there is an elevated risk of WMHACC. A variety of weldability tests have been developed over the years and are specifically designed to generate HACC by promoting special restraint conditions in the weld metal region [2,3,24,25]. Each test design develops specific restraint conditions and loading configurations so that their suitability to represent full-scale welding is not universal. A weldability test representative of pipeline girth welding for small diameter thin walled pipes, such as those typically found in the Australian context, must subject a girth weld deposited into a V-prep groove to high restraint conditions. Among the numerous weldability tests developed to date [3] the Welding Institute of Canada (WIC) test has proven to reproduce the restraint conditions during in-field pipeline girth welding. Nevertheless its short welding length and the traditionally deposited weld in a horizontal manual manner hinders the comparison between the weldability test result and the in-field conditions (vertical down 5G deposition).

The present work proposes an improved conception of the original WIC test into a novel geometry referred to as the 'Modified WIC' (MWIC) test. The improvement of the novel sample geometry is asserted by investigating girth welding conditions of gas transmission pipeline steel with cellulosic electrodes. It was considered imperative that any alteration to the sample design would not change the thermal field or the restraint conditions around the weld so that results obtained from samples with the altered design could be compared with those from the original design and with results from other laboratories.

## The traditional WIC weldability test

The WIC test [4,25–28] consists of depositing a single pass weld metal into a V-prep groove separating two restraint test plates. These plates are clamped with anchor welds to a stiffener tee with the restraint intensity controlled by the free-weld length (referred to as the restraint length) between the anchor welds (Figure 1). The welded joint is removed from the WIC specimen usually 24 h after welding completion by sawing the test assembly just inside the restraint length avoiding the ends of the anchor welds. The weld zone is then assessed for cracking.

Traditionally, the weld metal in the WIC test groove was deposited manually in the flat position. But this procedure has limited repeatability, originating from the variations in heat input inherent to manual welding. Moreover a vertical-down welding direction should be more representative of the in-field pipeline conditions. To reduce variations in the weld bead shape and heat input inherent with manual welding, a recent development of the WIC test procedure has included the mechanised vertical-down deposition of the weld metal to improve the consistency and repeatability of the tests [26].

In the WIC testing, the critical preheat temperature to avoid cracking depends on the welding conditions and weld metal chemistry, but also on the misalignment of the two welded plates [2]. This test has been

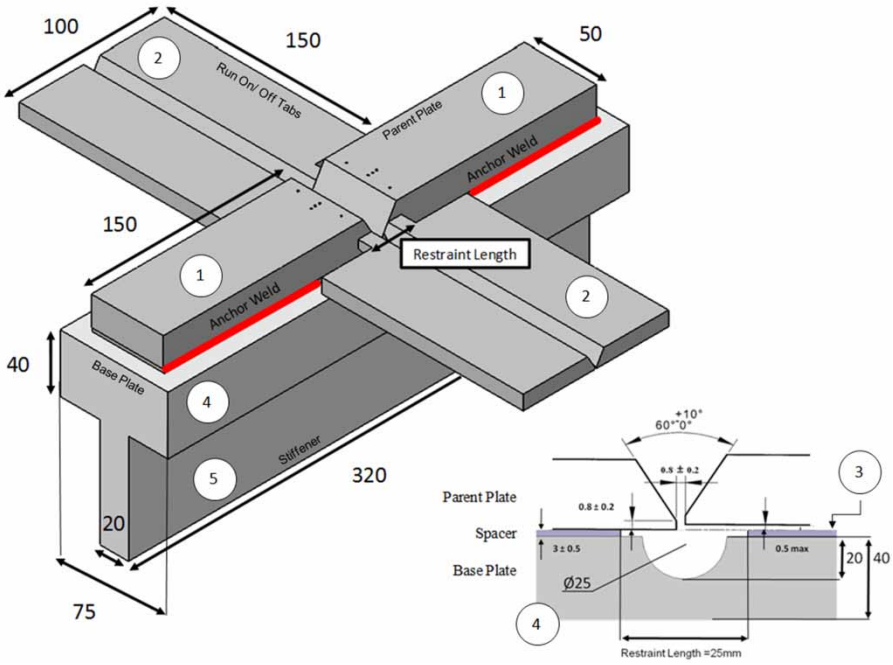


**Figure 2.** MWIC design. (1) Parent plate, (2) run on/off tab, (3) spacer, (4) tunnelled backing plate, (5) stiffener.

successful in comparing the HACC susceptibility of weld metals deposited by cellulosic Shielded metal arc welding (SMAW) consumables [4,27,29–33] and the critical preheat values to avoid cracking in the WIC test are similar to those obtained in full-scale weldability testing of pipe welding [27]. The WIC test has been benchmarked as a procedure for developing in-field pipeline welding requirements [34]. As both the critical preheat temperature and the restraint intensity affect crack formation, the critical restraint intensity-preheat temperature mapping concept was proposed to determine the thermo-mechanical conditions for cracking in the WIC test [4].

The traditional WIC test geometry has two major drawbacks in its geometry design: a short length for depositing the weld metal and the small gap between the backside of the groove root and the T-shaped support. The tests short test section (welding length) makes it difficult for a weld to be deposited under steady-state thermal conditions, leading to a strong influence of start and end conditions making the results difficult to interpret.

The small gap between the backside of the groove root and the T-shaped support which is provided by a 3 mm-thick spacer limits the access to the root of the weld. Such access is required for thermal analysis and local displacement measurement if the WIC test is to be instrumented. Moreover, this small gap hinders the venting of the gases produced during the decomposition of the electrode flux during SMAW. During in-field girth welding, large volumes of carbon monoxide and other shielding gases produced during welding flow through the weld keyhole into the pipe bore. The small back-space in the WIC test produces high back-pressures and causes the apparition of through-thickness holes in the weld metal. To compensate, a higher degree of welder compensation, in terms of lead angle, lateral weave and force with which the electrode is pushed into the weld prep to sustain the key hole, is required. Such a compensation results in a higher variation of heat input and is less representative of in-field welding conditions.

## The MWIC weldability test

The proposed geometric configuration of the MWIC Test was introduced after a series of iterative simulation and experimental studies aimed at improving the quality and consistency of the deposited weld bead [35]. The MWIC test has been designed (Figure 2) from the original geometric features of the WIC test. A 20 mm-diameter scoop is machined out below the welded joint to allow for the egress of the gases and dross. A change in the thickness of the backing plate from 20 to 40 mm ensures maintenance of the stiffness of the strong back. Run on and run off tabs, with the same V groove preparation as the test section, are TIG welded to the test plates (on one side) so as to follow the restraining movements of the test plates and not affect the restraint conditions. Access for instrumentation is also incorporated into the design (Figures 6 and 7).

## Finite element analysis

### *Simulation parameters*

To investigate the influence of the design modifications, geometrically representative models of the WIC and MWIC were created in a finite element modelling package; ANSYS® 14. Material properties of structural steel

**Table 1.** Material properties applied to the finite element simulation.

| | | | |
|---|---|---|---|
| Compressive yield strength | 250 MPa | Young's modulus | 200 GPa |
| Tensile yield strength | 250 MPa | Poisson's ratio | 0.3 |
| Tensile ultimate strength | 460 MPa | Bulk modulus | 167 GPa |

(Table 1) were applied to both specimens. Quad node shell elements were used for the structural analysis and tetrahedral solid heat transfer elements were used for the thermal analysis. The anchor welds were modelled as fixed supports and contact between the spacer, parent and backing plate was modelled though the use of contact elements. A coarse mesh was applied through the bulk of the geometry with a finer mesh applied in the region of interest.

## Restraint conditions

It is desirable for the MWIC test to have a similar deformation response under load to that of the WIC test, as this allows for cracking test results to be compared between the test specimens. Therefore, to compare the maximum displacement between nodes on the surfaces of the prepared edges of the WIC and MWIC tests a dimensionally accurate model of half of the tests were implemented. Symmetrical zero displacement boundary conditions were applied to simulate the sample being held in place on a flat surface. The restraint conditions of the MWIC and WIC specimens were investigated by applying a constant pressure to the weld area.

A stress of 300 MPa was applied on the surface of the root landing and the displacement of three nodes for WIC and MWIC, as illustrated in Figure 3, compared.

The calculated displacements for the three different nodes (in similar geometrical locations) in weld area for both original WIC and MWIC specimens are shown in Table 2. As expected the maximum displacements occurred in the *Z*-direction for both test specimens and this is due to the fact there is a tensile load applied in the *Z*-direction in the V groove (weld area). By comparing the results of the displacements for both samples (Table 2), for corresponding nodes, an increase of maximum 18.7% in displacement in the MWIC sample occurred in *Z*-direction. This suggests that the original WIC and the MWIC tests provide very similar restraint conditions.

**Table 2.** Comparison of displacements for the selected nodes in both WIC specimens (original and MWIC samples).

| | | Displacement µm | | |
|---|---|---|---|---|
| Coordinates | Nodes | WIC | MWIC | Comparison (%) |
| *X* | 1 | −0.12 | −0.13 | 9.6 |
| | 2 | −1.3 | −1.42 | 8.5 |
| | 3 | −2.7 | −3.12 | 8.9 |
| *Y* | 1 | 28.4 | 30.3 | 6.7 |
| | 2 | 25.9 | 28.0 | 8.1 |
| | 3 | 23.1 | 25.2 | 8.9 |
| *Z* | 1 | 44.4 | 51.9 | 17.0 |
| | 2 | 43.1 | 50.9 | 18.1 |
| | 3 | 42.1 | 50.0 | 18.7 |

## Thermal analysis

A 3D transient thermal analysis was conducted using a moving Gaussian heat source to compare the thermal response of the parent plate in the WIC and MWIC tests. The analysis methodology was similar to those employed by Darmadi et al. [36], Iacobescu [37], Teixeria et al. [38] and Alipooramirabad et al. [39]. The heat input was calculated in 0.1 s intervals for 8 s and distributed with a standard deviation of 1 mm and a mean that moved from one side to the other at a speed of 7 mm $s^{-1}$ along the weld surface. A coarse mesh was applied to reduce computational time due to the complexity of 3D transient thermal analyses with surface-surface radiation.

Simulation cases were run for single pass welds deposited at a heat input of 0.65 kJ $mm^{-1}$ on both 10

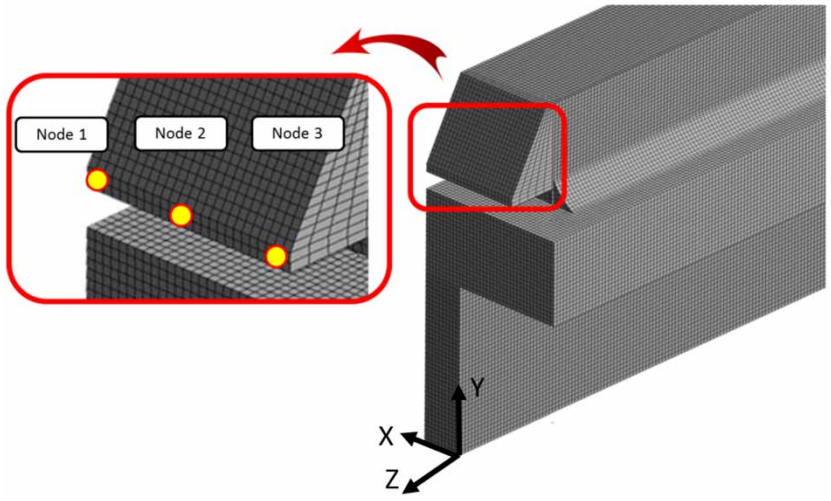


**Figure 3.** Schematic of relative position of nodes isolated for the analysis of displacement. The image highlights the position of the nodes isolated on the WIC test. For the MWIC test, nodes located in the sample position were used for the analysis.

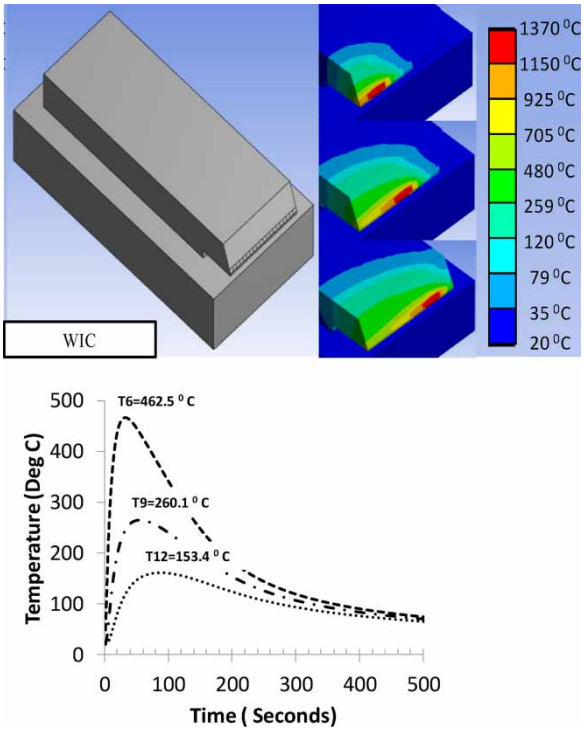


**Figure 4.** Thermal response of the standard WIC samples to local heating.

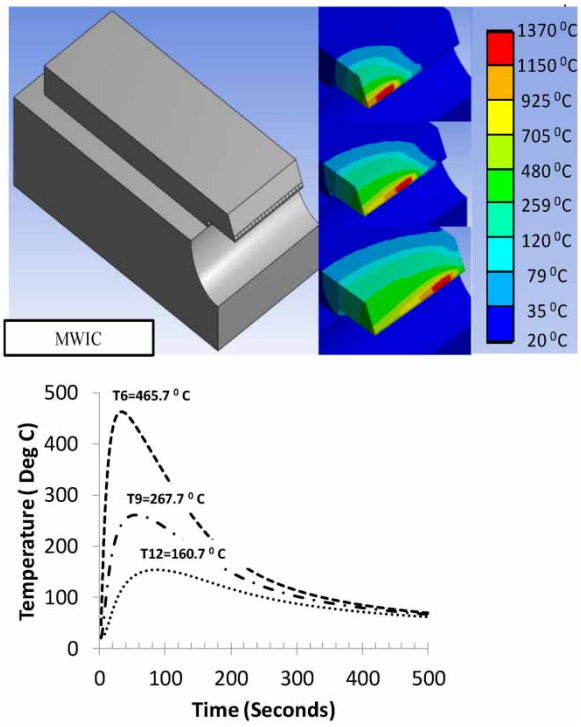


**Figure 5.** Thermal response of the MWIC samples to local heating.

and 20 mm thick parent plate. The heat input for the simulation case was selected as it is suggested to be representative of field conditions [40] and can be experimentally replicated for validation on both the WIC and MWIC tests. To compare the two specimens temperature probes are used to ascertain the peak temperature and cooling rates at 6, 9 and 12 mm away from the weld centreline. These positions correspond to the T6, T9 and T12 positions on the MWIC physical test specimen (Figure 6).

Figures 4 and 5 shows a typical temperature history during the welding cycle for the two designs at various distances from the weld axis. In the finite element calculations the typical temperature-dependent properties of steel were used and the local heating was modelled by an increase of the initial temperature in the weld location. The adopted simplifications are justified by the main objective of the modelling, which is to compare the thermal response of the two specimen geometries to the local intensive heating simulating to some extent the welding conditions. The accurate modelling of welding requires much greater computational effort and an extensive validation, which are outside of the scope of this paper.

The temperature fields presented in Figures 4 and 5 show a near negligible difference of the thermal responses to the local heating of the WIC and MWIC samples. For simulations run on 10 mm thick plate, the peak temperature difference between the WIC and MWIC tests was less than 7.5°C and for the 20 mm thick plate less than 5°C. The near negligible difference in recorded peak temperature and an approximate correlation coefficient of unity for all the positions (T6, T9 and T12) with regards of the cooling rates suggests the specimens are comparable from a thermal perspective.

## Weldability testing

To establish the performance of the MWIC test a two tier experimental programme was employed as summarised in Table 3.

### *Testing parameters*

Weldability testing was carried out on a uni-directional, mechanised SMA welding machine with a specimen-holding plate moving vertically upwards during welding at a controlled velocity, thus simulating vertical-down welding conditions. Welding parameters are

**Table 3.** Divisions of the experimental programme.

| | |
|---|---|
| Tier 1 | ***Experimental validation of simulation results and design modifications***<br>A series of weldability tests were conducted on the WIC and MWIC test specimen, replicating conditions that were simulated using FEA. The primary objective of Tier 1 testing is to validate the comparability of the thermal response of the two test specimens |
| Tier 2 | ***Comparative weldability envelope evaluation***<br>Weldability tests were conducted for a broad range of parameters on the WIC and MWIC test to provide a sample set with which the deposition window can be compared. Additionally the sample set provides the basis to compare repeatability and reliability of the test specimens. |

**Table 4.** Welding parameters.

| Welding specifications | | Welding parameters | |
|---|---|---|---|
| Direction | Vertical down (5G) | Current | 130–170 A |
| Size of electrode | 4.0 mm | Voltage | 25–30 V |
| AWS class | A5.1 | Travel speed | 250–470 mm $min^{-1}$ |
| Specification | E6010 | Heat input range | 0.41–1.00 kJ $mm^{-1}$ |
| Polarity | DC+ | Preheat range | 25–100°C |

summarised in Table 4. A constant force and an angle of 20° normal to the plate were maintained between the electrode and the workpiece. The Lincoln Electric Invertec 350V Pro was used as the welding power source. The groove surfaces of the test specimen and 25 mm either side of the weld centreline was polished down with ISO 80 grit (201 µm) emery paper and degreased with acetone. The entire specimen was degaussed prior to welding. The WIC and MWIC specimen designs were tested across a heat input range (0.4–1.0 kJ $mm^{-1}$), using commonly encountered welding parameters when laying the root pass of a girth weld (Table 4).

## Material

The WIC and MWIC tests were fabricated using API 5L grade X70 line pipe steel for test plate. The weld deposition was performed with a 4 mm-diameter E6010 electrodes. The test plate chemical composition is given in Table 5 and the electrodes batch chemistry is given in Table 6.

## Thermal analysis

Test plate thermal data was obtained by fitting three electrically-grounded K-type thermocouples (1 mm outer diameter) coated with thermal paste into the parent plate. The three 1.2 mm diameter holes are 1 mm off the bottom of the parent plate and 6 (T6), 9 (T9) and 12 (T12) mm away from the weld centreline, respectively (Figure 6). This allows for measurement of the thermal cycle from HAZ through to the unaffected base metal. Two additional thermocouple access holes, the top tracker (TT) and bottom tracker (BT) were drilled 5 mm from the edge of test section (1 mm off the bottom surface) to measure the entry and exit temperature of the test section to verify relative thermal homogeneity in the test weld.

The weld metal centreline temperature was measured through an access port drilled through the tunnelled backing plate (Figure 7). An R-type thermocouple was plunged into the molten weld pool through the centreline access port at the specimens' back, behind the welding arc without interfering with the welding process (Figure 7).

## Local strain measurement

Ideally, what is most pertinent to cracking is the strain experienced by the weld metal from its deposition and during its solidification and cooling. In this study, the strain was measured using an extensometer in the local vicinity of the weld. The deformation of the weld metal will capture the local displacement (at the weld metal

**Table 5.** Chemical composition of line pipe steel (% weight) (from manufacturer).

| C | Mn | Si | S | P | Nb | Ti | Cu | Ni | Mo | Cr | Ca | Al | V |
|---|---|---|---|---|---|---|---|---|---|---|---|---|---|
| 0.052 | 1.55 | 0.21 | 0.0011 | 0.0097 | 0.041 | 0.012 | 0.15 | 0.19 | 0.18 | 0.026 | 0.0016 | 0.039 | 0.029 |

**Table 6.** Electrode batch chemical composition (% weight) (from manufacturer).

| C | Mn | Si | S | P | Ni | Mo | Cr | V |
|---|---|---|---|---|---|---|---|---|
| 0.16 | 0.62 | 0.19 | 0.009 | 0.009 | 0.2 | 0.01 | 0.02 | < 0.01 |

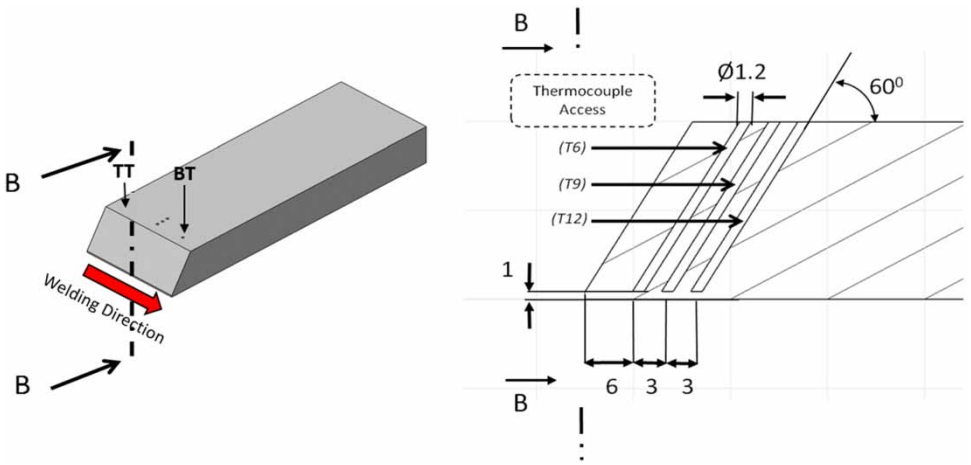


**Figure 6.** Isometric and cross-sectional view of thermocouple access for parent plate.

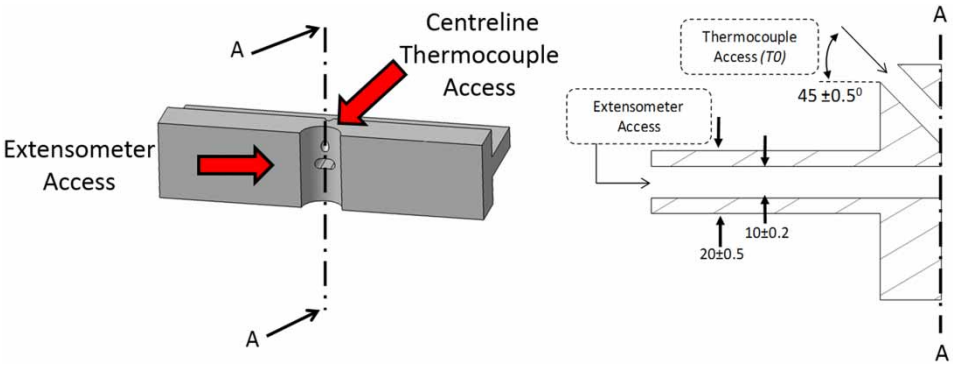


**Figure 7.** Isometric and cross-sectional view of instrumentation access for weld centreline temperature and local weld metal displacement.

scale) and allow for a measure of the residual stress that builds up until the attainment of the room temperature by the weldment. A high temperature extensometer (Epsilon 3448-10-50) was attached underneath the weld coupon, through the drilled access shown in Figure 7, in the path of the weld at mid-length, to measure the local transverse strain across the weld pool during and after the welding process. The gauge length of the extensometer is 10 mm spanning across a 6 mm-wide weld bead.

### *Data acquisition*

The extensometer and thermocouples outputs were filtered and recorded at a 10 Hz frequency during the entire test using a Virtual Instrument built using Lab View®-2010. The data signals are acquired through a NI-CDAQ-9188 analog-to-digital converter and channelled through an optical isolation system into several 16bit National Instruments® (NI) 9215 voltage modules embedded in a NI-CDAQ-9188 chassis. Welding voltage and current was recorded at 2 Hz using Lincoln Electrics® (LE) proprietary software; LE Power Wave Manager.

### *Weld analysis*

The welded joint was removed from the WIC and MWIC specimens 24 h after weld completion by milling the test assembly just inside the restraint length. The anchor welds were sawed off using a water-cooled precision metallographic saw. The weld zone was assessed for cracking by examining six weld metal transverse cross-sections prepared for metallurgical inspection (Figure 8). A sample is defined as cracked (Figure 9) if a planner defect is visually identified on a sample surface when magnified at ×400, and the vertical length of the defect is greater than 5% of the height of the weld bead ($t_w$). The weld metal microstructure was examined using an optical microscope on metallographically prepared weldments cross-sections, (polished to 1 µm diamond paste and etched in a 2% nital solution).

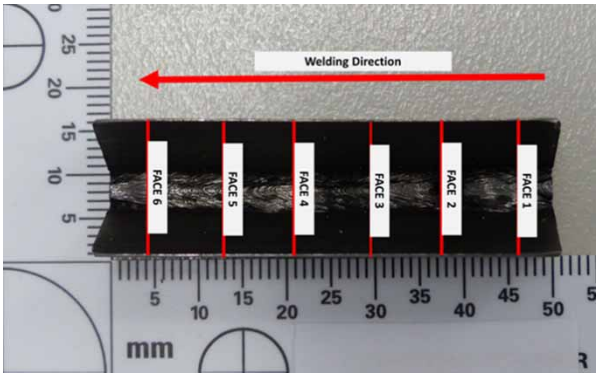


**Figure 8.** Weldability testpiece with the location of the six faces to be examined under an optical microscope at a magnification of ×400.

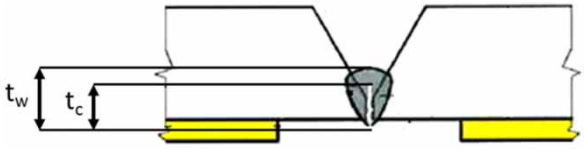


**Figure 9.** Schematic of a face of a test section. A sample is defined as cracked when a linear defect whose vertical length ($t_c$) is greater than 5% of the bead height ($t_w$).

## Results

### *Tier 1: Experimental validation of simulated results and design modifications*

#### *Thermal results*

Experimental cooling rates and peak temperature data showed a strong positive correlation with simulated results for the WIC and MWIC tests. A maximum difference of 58°C in peak temperature was noted between simulated and experiential results. This difference can be accounted for by the simplifications, including the use of coarse mesh, employed when constructing the

**Table 7.** Comparison of the peak temperatures for 20 mm thick MWIC and WIC tests at $0.85 \pm 0.02$ kJ mm$^{-1}$ under ambient conditions and maximum restraint.

| | Peak temperature (°C) | | | | |
|---|---|---|---|---|---|
| Sample | TT | T6 | T9 | T12 | BT |
| MWIC | 402°C | 384°C | 251°C | 175°C | 375°C |
| WIC | 425°C | 416°C | 266°C | 184°C | 401°C |
| % Difference | 5.7% | 8.3% | 5.9% | 5.1% | 6.9% |

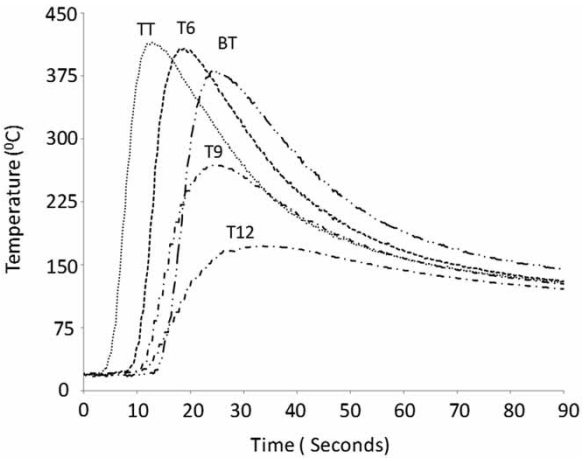


**Figure 10.** Mean thermal profile of 20 mm thick MWIC at tests at $0.85 \pm 0.02$ kJ mm$^{-1}$ under ambient conditions ($25 \pm 5$°C) and maximum restraint.

thermal model. Nevertheless the recorded temperature differences between the WIC and MWIC parent was less than 8.5% (Table 7). Temperature measurements taken from the TT and BT thermocouples on the MWIC show similar cooling rates indicating a high degree of thermal homogeneity within the test section and verifying that the run on tabs have no effect on the cooling rates at the edge of the test section. Figure 10 illustrates the mean temperature profile of MWIC tests carried out at $0.85 \pm 0.02$ kJ mm$^{-1}$ under ambient conditions ($25 \pm 5$°C) and maximum restraint. Across the entire range of experiments there was less than 10% difference in the peak temperatures recorded. This variance was random and could be attributed to experimental error introduced as a result of contact and response time of the thermocouple with the parent plate.

To establish the thermal cracking index, incorporating the critical cooling time $t_{8/5}$ under various welding conditions, an R-type thermocouple was lanced into the molten weld pool behind the arc. Given the intrinsic geometric configuration of the traditional WIC test this was not possible without disturbing the test sequence. However, the rear access port on the MWIC test allowed for successful plunging in. Measurements on weld metals without (Figure 11) and with (Figure 12) plunged thermocouples highlight an increase in hardness values for the latter experimental condition. This hardness increase is possibly related to different cooling conditions and elemental contaminations from the thermocouples. Indeed, EDX scans on weld metal with plunged thermocouples revealed traces of platinum (Pt) and rhodium (Rh) in the weld pool (Figure 13), thus potentially distorting any conclusion drawing when using the MWIC weldability test or for that matter any weldability test that had a thermocouple plunged into the molten weld pool.

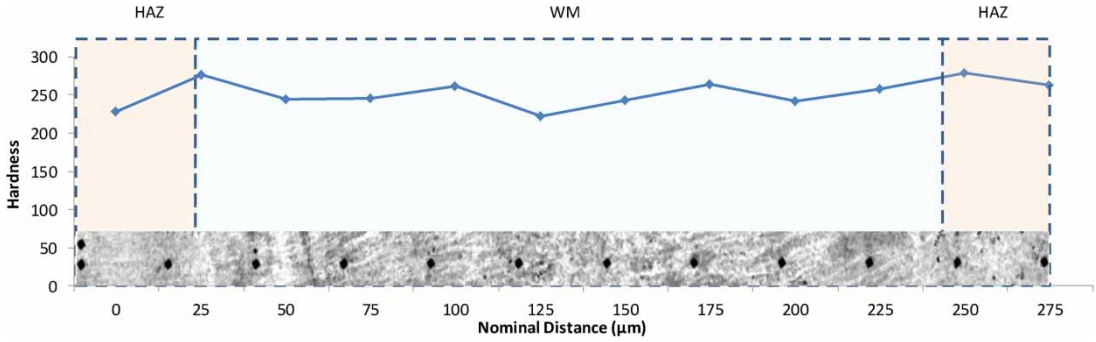


**Figure 11.** Weld metal harness traverse for MWIC sample without a thermocouple plunge and consequently expected hardness levels.

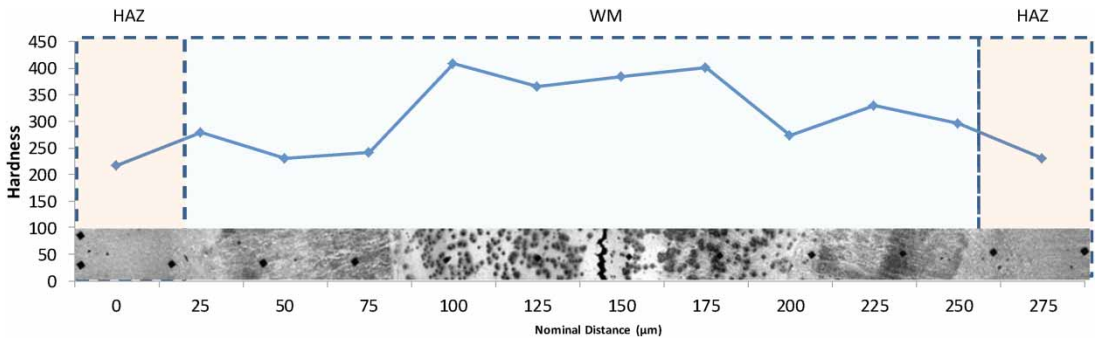


**Figure 12.** Weld metal hardness traverse for MWIC sample with R-type thermocouple plunged and consequent elevated hardness.

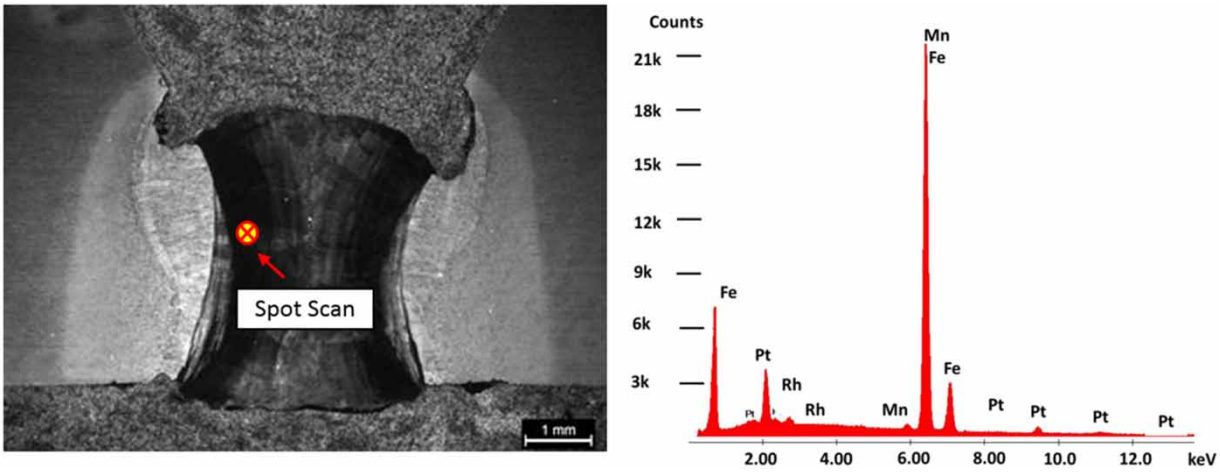


**Figure 13.** Plunged sample Le Pera's etching macrograph (left). EDX spectrum of spot scan at 20 kV (right).

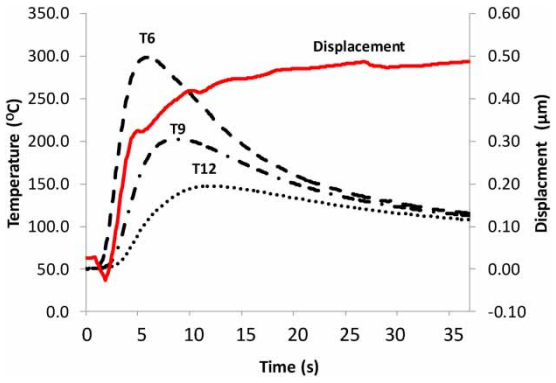


**Figure 14.** Strain measurement superposed to thermal analyses for a MWIC test under experimental conditions: 20 mm thick baseplates, 0.6 kJ mm$^{-1}$ heat input, 50 ± 5°C preheat, 50 mm restraint length.

### *Displacement results*

An extensometer of 10-mm gauge length is spanned across the groove prior to welding on the root side. An example of strain measurement made during the MWIC test is presented in Figure 14, shown as a function of time with the thermal analysis superimposed. Negative strain represents displacement toward the weld centreline. Note that the strain becomes negative between 1 and 4 s, which is likely due to thermal expansion ahead of the advancing weld electrode [41]. The irregularity of the strain curve likely represents intermittent crack growth, in agreement with the observations of other researchers [4,42]. Restraint length affects local strain even for uncracked welds. This could be due to the lower cooling rate at longer restraint length resulting in lower rates of solidification shrinkage and thermal contraction.

## *Tier 2: Weldability envelope evaluation*

### *Deposition envelope*

Welding trials showed that for 20 mm thick plates under ambient conditions, at heat inputs lower than 0.45 kJ mm$^{-1}$ both tests produced defective welds that exhibited lack of fusion and penetration. Testing results also showed that the MWIC specimen could be used to deposit defect free welds between 0.5 and 1.0 kJ mm$^{-1}$, whereas the standard WIC test was limited to a heat input range of above 0.8 kJ mm$^{-1}$ (Figure 15). Welds deposited on the WIC specimen below this range resulted in the formation of 'windows' to the point where the weld did not represent field weld quality and would generate undue stress concentration for accurate determination for the onset of HACC (Figure 16).

Welding in the WIC and MWIC test proved the existence of a lower limit in welding heat inputs. However, while defective welds were deposited in the WIC test below 0.9 kJ mm$^{-1}$, the MWIC test deposited acceptable welds as low as 0.5 kJ mm$^{-1}$. Figure 16 highlights the considered defective welds.

### *Weld bead consistency*

The weld profile for the WIC and the MWIC were compared at the heat input range where both tests could successfully deposit a defect free weld (Figure 17). The mean throat thickness for the 12 examined sections of the WIC test ranged from 4.5 to 6 mm, whereas for the MWIC test ranged from 5.5 to 5.7 mm. The MWIC tests showed less than 10% variation in mean throat thickness across the range of heat inputs tested (0.5–1.0 kJ mm$^{-1}$).

## Discussion

A weld metal cold cracking is formed if a hydrogenated susceptible microstructure is subjected to a stress greater than a threshold value. The WIC and MWIC test can both be used to rank single pass welds in regards to their susceptibility to cold cracking for a range of welding parameters, preheats, consumable and parent plate chemistries.

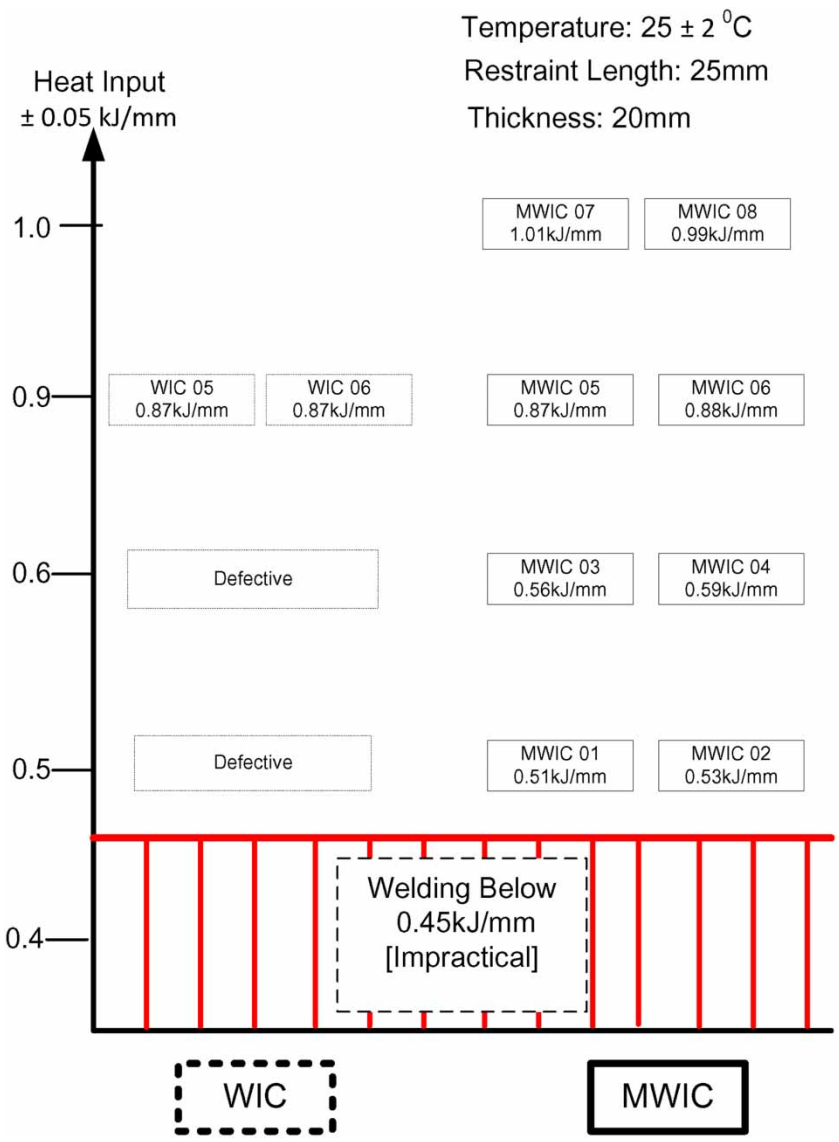


**Figure 15.** Weldability test range for the WIC and MWIC specimens across the root pass heat input range.

The heat input range representative of the root pass conditions encountered on a pipeline spread corresponds to low heat inputs due to fast welding speeds. While the WIC test has been cited extensively in literature as a tool to prescribe the critical preheat required to avoid cracking [2], the MWIC test possesses modifications of the WIC test that enhance the tests suitability at low heat inputs and high travel speeds. Experimental results demonstrated the MWIC test can be employed with confidence in the heat input range from 0.5 to 1 kJ $mm^{-1}$ where the traditional WIC test cannot (Figure 18).

The MWIC test produces welds with a more consistent throat thickness than the WIC test, improving the reliability and repeatability of the tests. The WIC test and by extension the MWIC test allows for a variation in restraint through the variation in the length of the anchor welds, and thus for the quantification of the critical restraint needed to initiate cracking. However, asymmetry in the weld profile and inconsistency in the throat thickness common with the traditional WIC test promotes scatter in identification of the crack/no crack boundary. The modifications to the WIC test reduced the variation in throat thickness and improved the sensitivity of the test. To illustrate the point consider Figures 19 and 20. MWIC_01 and MWIC_02 were welded within ±0.05 kJ $mm^{-1}$ of each other. Both tests showed similar cracking characteristics in terms of the location of the crack and size of the crack across the sections examined suggesting an enhancement in the reliability of the test.

Finally the MWIC test has been instrumented to give access to the weld metal thermal history and displacement data. Thermal analysis provides the input to estimate the validity of the use of $t_{8/1}$ criteria. The thermocouple access allows for a thermocouple to be plunged into the molten weld pool giving access to the complete thermal history of the weld metal. Extraction of the $t_{8/5}$ can be linked to the resulting microstructure, $t_{100}$ to the diffusible hydrogen content and local weld

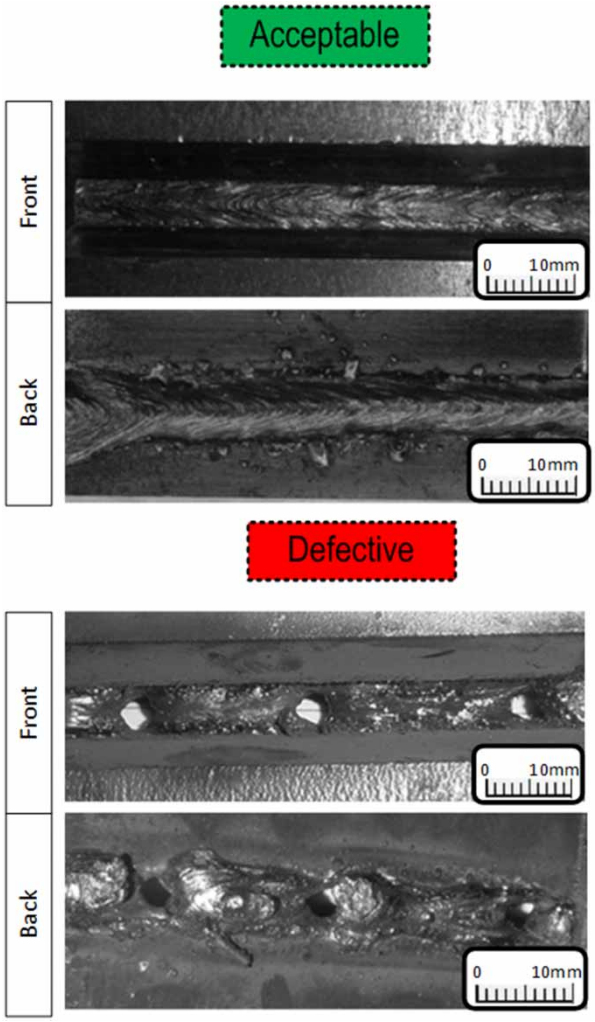


**Figure 16.** Acceptable and defective welds highlighting the defective welding 'window'/burn through on the WIC test at low heat input and high travel speed.

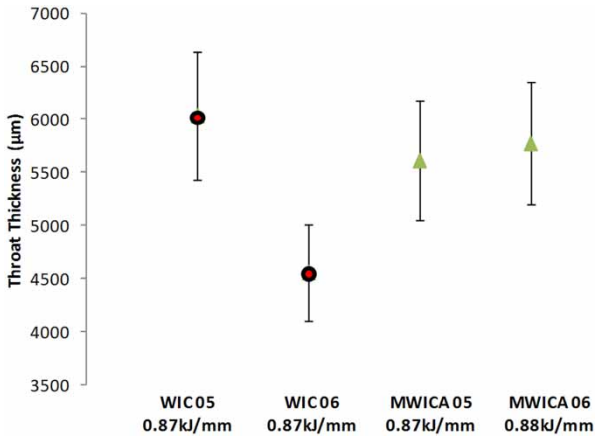


**Figure 17.** Comparison weld throat thickness for WIC and MWIC tests at $0.85 \pm 0.02$ kJ mm$^{-1}$.

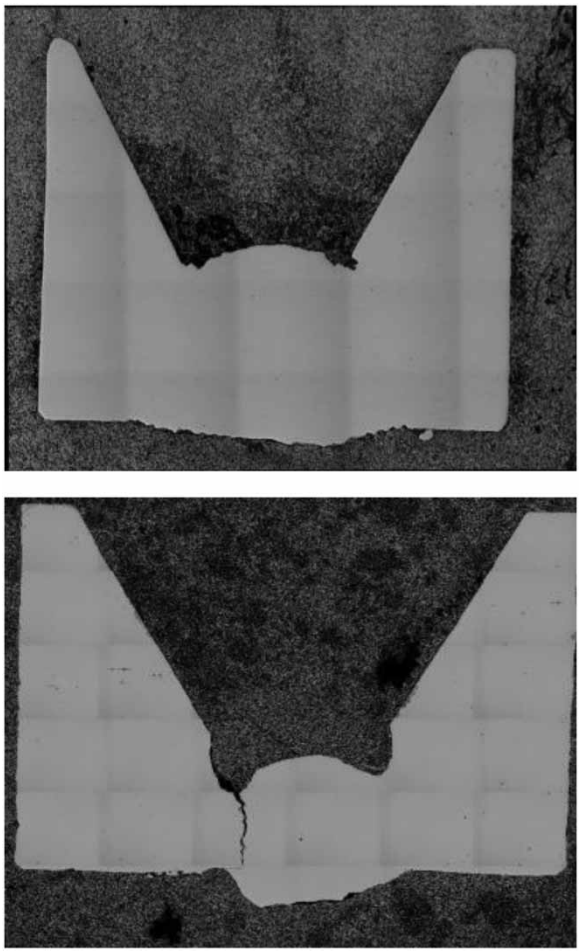

**Figure 18.** Typical symmetric (top) and asymmetric (bottom) weld bead profile. (*Images not to scale*).

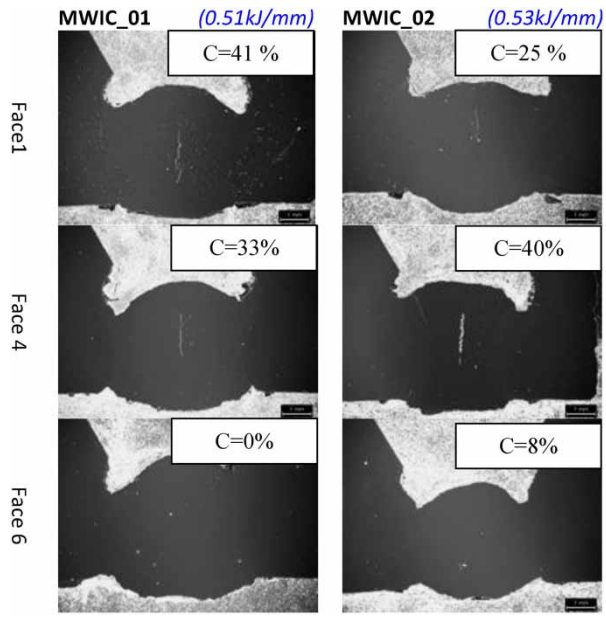


**Figure 19.** MWIC cracking results for tests carried out at $0.5 \pm 0.05$ kJ mm$^{-1}$ on 20 mm $\times$70 plate. Percentage cracking is calculated as; (C%) = [Crack length ($t_c$)/Throat thickness ($t_W$)] $\times$ 100.

metal displacement to resulting strain. Collectively this data can be used as a proxy to quantify the three critical factors driving HACC.

Assuming that all thermo-metallurgical factors are held constant (e.g. constant alloy composition and cooling rate), it is useful to concentrate on the thermo-mechanical conditions require for crack formation. Measuring local strain in the vicinity of the weld during

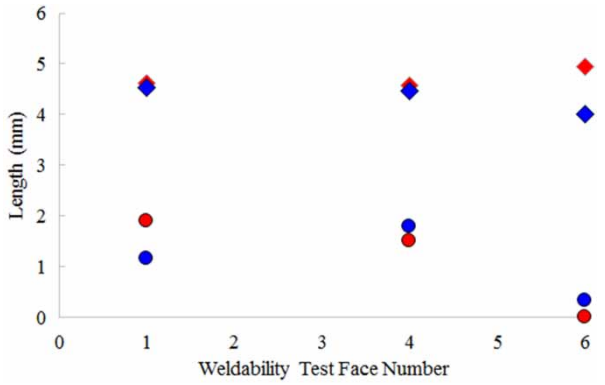


**Figure 20.** Variation in $t_w$ for MWIC_01 (◆) and MWIC_02 (◆) and $t_c$ for MWIC_01 (●) and MWIC_02 (●).

the whole welding cycle poses some unique challenges such as the high temperatures encountered in welding. The hole drilled through the back of the T-support enables the access of an extensometer and strain measurements that are lacking today.

## Conclusions

A new MWIC weldability test and test procedure have been developed that allows for the experimental determination of the critical strain needed for cold cracking formation post-welding. In particular the weldability of API-5L-X70 was examined for E6010 cellulosic SMA weld metal. The modifications allowed obtaining a significant increase in success rate of achieving an industry acceptable weld in the tests. The new designed geometry enables easier access for instrumentation and for the more reproducible production of test specimens facilitating the use of the test specimen as a research tool. To ensure that the modifications did not modify significantly the thermal and restraint conditions of the test and the results are comparable with those achieved in other studies using the WIC test, physical and finite element studies for the original and modified test geometries have been undertaken. The results show that the modifications to the design have little or no influence on the thermal and mechanical properties of the test, but improve the ease with which consistently high quality samples are produced.

Although the MWIC test is in some regards similar to the WIC test in its application of controlled transverse global restraint levels, what is of particular importance in the MWIC test is the measurement of local strain critical to crack formation. The same approach could be accomplished using other established weldability tests including tensile tests (e.g. TRC) or restraint applied in the plane of the test specimen (e.g. RRC, window type cruciform test, H-slit test, Lehigh slot test) [2,3]. Weldability tests that do not lend to themselves to this approach are those involving bending, where the strain is not uniform throughout the test specimen. The disadvantage of the strain analysis is that it adds to test complexity and is time consuming. However, expressing cracking susceptibility in terms of a critical parameter directly related to a cracking mechanism has the advantage of providing a more meaningful representation of weldability. Of particular importance is the possibility to use these data in the modelling of cracking mechanisms, allowing for future prediction. Strain analysis also allows for the identification of the instance of crack formation, thus possibly identifying if solidification cracking has formed prior to HACC formation.

## Acknowledgements

The research work was funded by the Energy Pipeline CRC supported through the Australian Government's Cooperative Research Centres Program. The cash and in-kind support from the APIA-RSC is gratefully acknowledged. The authors would like to thank Neville Cornish, Principle Welding Engineer, Australian Welding Solutions (AWS) for access to welding facilities and Pascal Symons, Welding Technician, University of Adelaide. We would also like to thank Prof V Linton of the Energy Pipeline CRC for her continued support and A/Prof A. Kotousov, Dr E. Gamboa, I. Brown and PhD candidates Walter Costin and Houman Alipooramirabad for their comments and discussion. Adelaide Microscopy and Technical team are also gratefully acknowledged.

## Disclosure statement

No potential conflict of interest was reported by the authors.

## References

[1] Yurioka N. Predictive methods for prevention and control of hydrogen assisted cold cracking. First international conference on 'weld metal hydrogen cracking in pipeline grith welds'; 1999; Wollongong, Australia.
[2] Yurioka N, Suzuki H. Hydrogen assisted cracking in C-Mn and low alloy steel weldments. Int Mater Rev. 1990;35(4):217–249.
[3] Kannengiesser T, Boellinghaus T. Cold cracking tests – an overview of present technologies and applications. Weld World. 2013;57(1):3–37.
[4] Alam N, Dunne D, Barbaro FJ. Weld metal crack testing for high strength cellulosic electrodes. First international conference on 'weld metal hydrogen cracking in pipeline girth welds'; 1999; WTIA, Wollongong, Australia. p 9.1–9.23.
[5] Barbaro FJ. Types of hydrogen cracking in pipeline girth welds. First international conference on 'weld metal hydrogen cracking in pipeline girth welds'; 1999; WTIA, Wollongong, Australia. p. 11.1–11.15.
[6] Costin W, Lavigne O, Linton VM, et al. Micromechanical examination of the relationship between weld metal microstructure and hydrogen assisted cold cracking. 6th International Pipeline Technology Conference; 2013 Oct 6–9; Ostend, Belgium.
[7] Costin WL, Lavigne O, Kotousov A, et al. Investigation of hydrogen assisted cracking in acicular ferrite using site-specific micro-fracture tests. Mater Sci Eng A. 2016;651:859–868.
[8] ASNZS 2885.2-2008 Pipelines – Gas and liquid petroleum Part 2 – Welding; 2007; Australia.

[9] BS EN 1011-2:2001 Welding. Recommendations for welding of metallic materials. Arc welding of ferritic steels.
[10] Eliaz N, Eliezer D, Olson DL. Hydrogen-assisted processing of materials. Mater Sci Eng A. 2000;289(1–2): 41–53.
[11] Bailey N. Weldability of ferritic steels. Abington, UK: Woodhead Publishing Ltd; 1994.
[12] Bailey N, Coe FR, Gooch TG, et al. Welding without hydrogen cracking. 2nd edn. Cambridge: TWI, Abington Publishing; 1995.
[13] Davidson JA, Konkol PJ, Sovak JF. Assessing fracture toughness and cracking susceptibility of steel weldments—a review. Weld Res Coun Bull. 1989;45(345): 1–43.
[14] Lynch S. Hydrogen embrittlement phenomena and mechanisms. Corros Rev. 2012;30:105–123.
[15] Smialowski M. Hydrogen in steel. Oxford: Pergamon Press Ltd; 1962.
[16] Fletcher L. Field weldability of large-diameter thick-walled linepipe. Aust Weld J. 1988;First Quarter(17): 17–21.
[17] Fletcher L, Yurioka N. A holistic model of hydrogen cracking in pipeline girth welds. First international conference on 'weld metal hydrogen cracking in pipeline girth welds'; 1999; Wollongong, Australia.
[18] Kotousov A, Borkowski K, Fletcher L, et al. A model of hydrogen assisted cold cracking in weld metal. 9th international pipeline conference; 2012; Calgary, Alberta, Canada, ASME.
[19] Roshan W, Bumpstead M, Fletcher L, et al. Welding of small diameter pipelines in Australia. APIA/EPRG/PRCI 19th Joint Technical Meeting; 2013; Sydney, Australia.
[20] Kumar PG, Yu-ichi K. Diffusible hydrogen in steel weldments. Trans JWRI. 2013;42:39–62.
[21] Alipooramirabad H, Ghomashchi R, Paradowska A, et al. Residual stress-microstructure-mechanical property interrelationships in multipass HSLA steel welds. J Mater Process Technol. 2016;231:456–467.
[22] Radaj D. Heat effects of welding: temperature field, residual stress, distortion. Berlin: Springer-Verlag; 2012.
[23] Satoh K, Terasaki T, Ohkuma Y. Relationship between critical stress of HAZ cracking and residual diffusible hydrogen content. J Japan Weld Soc. 1979;48(4):248–252.
[24] Graville BA. A survey review of weld metal hydrogen cracking. Weld World. 1986;24(9/10):190–198.
[25] Graville BA. Interpretive report on weldability tests for hydrogen cracking of higher strength steels and their potential for standardization. New York: NY, Welding Research Council, New York; 1995.
[26] Coniglio N, Barbaro FJ, Linton VM, et al. Hydrogen assisted cold cracking susceptibility of weld metal deposited by cellulosic shielded metal arc welding consumables. International pipeline conference, IPC2010; 2010; Calgary, Canada.
[27] North TH, Rothwell B, Glover A, et al. Weldability of high strength line pipe steels. Weld J. 1982;61(8): 243–257.
[28] Signes EG, Howe P. Hydrogen-assisted cracking in high-strength pipeline steels. Weld J. 1988;67(8):163s–170s.
[29] Lazor RB, Graville B. Effect of microalloying on weld cracking in low carbon steels. Canadian Welder Fabricator. 1983;74(21):21–23.
[30] Sarrafan S, Ghaini FM, Rahimi E. Weld metal hydrogen cracking in transmission pipelines construction. Proceedings of the 8th international pipeline conference IPC2010; 2010; Calgary, Canada.
[31] Cola MJ. Investigation of WIC test variables. Houston, TX: Edison Welding Institute; 1991.
[32] Lazor RB. Examination of pipeline welding procedural variables. Houston, TX: Pipeline Research Council International; 1984.
[33] Noble DN, Pargeter RJ. Field weldability of high strength pipeline steels. Houston, TX: Edison Welding Institute; 1988.
[34] Glover A, Rothwell B. Specifications and practices for hydrogen crack avoidance in pipeline girth welds. First international conference on 'weld metal hydrogen cracking in pipeline girth welds'; 1999; WTIA: Wollongong, Australia. p. 13.1–13.18.
[35] Kurji R. Thermo mechanical factors influencing weld metal hydrogen assisted cold cracking. School of Mechanical Engineering. PhD Project, The University of Adelaide: Adelaide, Australia; 2016.
[36] Darmadi D, Norrish J, Tieu AK. Analytic and finite element solutions for temperature profiles in welding using varied heat source models. World Acad Sci Eng Technol. 2011;81:154–162.
[37] Iacobescu G. A theoretical model for welding process with Gaussian heat source – Part 1. Univ 'Politehnica' Bucharest Sci Bull, Series D: Mech Eng. 2006;68(4): 45–50.
[38] Teixeira PRDF, Araújo DBD, Cunda LABD. Study of the Gaussian distribution heat source model applied to numerical thermal simulations of TIG welding processes; 2014.
[39] Alipooramirabad H, Paradowska AM, Ghomashchi R, et al. Prediction of welding stresses in WIC test and its application in pipelines. Mater Sci Technol. 2016;32(14):1462–1470.
[40] Kurji R, Coniglio N, Gamboa E, Ghomashchi R. Weld metal HACC susceptibility under controlled welding conditions and restraint levels. Adelaide, Australia: Energy Pipeline CRC; 2011.
[41] Chihoski RA. The character of stress fields around a weld arc moving on aluminum sheet. Weld J. 1972;51(1):9–18.
[42] Vasudevan R, Stout RD, Pense AW. Hydrogen-assisted cracking in HSLA pipeline steels. Weld Res Suppl. 1981;60(9):155–168.